Solution structure of the TatB component of the twin-arginine translocation system

Yi Zhang [a,b], Lei Wang [a,b], Yunfei Hu [a,c],*, Changwen Jin [a,b,c],**

[a] Beijing Nuclear Magnetic Resonance Center, Peking University, Beijing 100871, China
[b] College of Life Sciences, Peking University, Beijing 100871, China
[c] College of Chemistry and Molecular Engineering, Peking University, Beijing 100871, China

ARTICLE INFO

ABSTRACT

The twin-arginine protein transport (Tat) system translocates fully folded proteins across lipid membranes. In *Escherichia coli*, the Tat system comprises three essential components: TatA, TatB and TatC. The protein translocation process is proposed to initiate by signal peptide recognition and substrate binding to the TatBC complex. Upon formation of the TatBC–substrate protein complex, the TatA subunits are recruited and form the protein translocation pore. Experimental evidences suggest that TatB forms a tight complex with TatC at 1:1 molar ratio and the TatBC complex contains multiple copies of both proteins. Cross-linking experiments demonstrate that TatB functions in tetrameric units and interacts with both TatC and substrate proteins. However, structural information of the TatB protein is still lacking, and its functional mechanism remains elusive. Herein, we report the solution structure of TatB in DPC micelles determined by Nuclear Magnetic Resonance (NMR) spectroscopy. Overall, the structure shows an extended 'L-shape' conformation comprising four helices: a transmembrane helix (TMH) $\alpha 1$, an amphipathic helix (APH) $\alpha 2$, and two solvent exposed helices $\alpha 3$ and $\alpha 4$. The packing of TMH and APH is relatively rigid, whereas helices $\alpha 3$ and $\alpha 4$ display notably higher mobility. The observed floppiness of helices $\alpha 3$ and $\alpha 4$ allows TatB to sample a large conformational space, thus providing high structural plasticity to interact with substrate proteins of different sizes and shapes.

1. Introduction

Protein translocation across lipid membranes is mainly accomplished by the Sec or twin-arginine translocation (Tat) protein transport systems [1]. The Sec system is ubiquitous in all organisms and translocates substrate proteins in an unfolded state via a threading mechanism. The Tat system, on the other hand, is a unique protein translocation system identified in bacteria, plant chloroplasts and archaea [2]. The main characteristic of this system is its ability to translocate proteins in their fully folded states, sometimes with bound cofactors or even in oligomeric forms [2,3]. Many substrates of this system are virulence factors for pathogens, bacteria, and other substrates that play essential

roles for bacteria under stress conditions [4]. Therefore, elucidating the molecular mechanism of the Tat system would provide valuable insights for anti-bacterial drug design.

In gram-negative bacteria such as *Escherichia coli*, the Tat system consists of three essential components: TatA, TatB and TatC. The TatA component is believed to form the protein translocation pore via self-oligomerization [5–8]. The TatB protein is a paralog of TatA. It forms a complex with TatC and functions together in substrate recognition and binding [9–14]. Several models for the Tat translocation mechanism have been proposed [2]. The commonly accepted mechanism suggests that the transportation cycle is initiated by the binding of the signal peptide to the TatBC complex [2,15,16]. In this step, TatC recognizes the signal peptide containing the conserved SRRXFLK motif while the substrate protein is positioned in the vicinity of TatB [2]. Next, the proton motive force (PMF) strengthens the binding and recruits the TatA subunits, which subsequently form into the translocation channel by self-oligomerization [2]. Finally, the substrate is transported across the membrane and the TatA channel dissociates, completing one cycle of the translocation [17–19].

Recently, high-resolution structural studies provided valuable insights into the functions of TatA and TatC subunits [8,10,20]. However, the structure of TatB remains unknown. The TatB protein adopts an N-out topology in cells [21]. It functions in a tetrameric state in the

TatBC complex and protects the signal peptides from being cleaved before translocation [22,23]. The lack of structural information of the TatB subunit hinders deeper understanding of the molecular mechanism of its function in the Tat translocation process.

Herein, we report the structural and dynamic studies of *E. coli* TatB by NMR spectroscopy. We show that TatB adopts an extended L-shape conformation comprising four helices: a single transmembrane helix (TMH), an amphipathic helix (APH) and another two hydrophilic helices in the C-terminal region. Furthermore, backbone dynamics indicates that the two hydrophilic helices at the C-terminus display a relatively high mobility, which may facilitate binding to substrate proteins with different sizes and shapes. Our current study provides structural insights into understanding the molecular mechanism of TatB function during translocation.

2. Materials and methods

2.1. Sample preparation

The gene encoding residues Met1–Pro101 of *E. coli* TatB was cloned into the pET21a(+) vector (Novagen) and expressed in *E. coli* BL21 strain (Stratagen) with a C-terminal fused 6× His tag. The cell culture was grown overnight in 4 mL Luria–Bertani medium at 35 °C, then centrifuged and resuspended in 200 mL M9 minimal medium. For the production of $^{13}C/^{15}N$- or ^{15}N-labeled samples, $^{15}NH_4Cl$ and $^{13}C_6$-glucose were used in the M9 medium. When OD_{600} reached 0.8, isopropyl-β-D-thiogalactoside (IPTG) was added to a final concentration of 40 mg/L to induce protein expression. The cells were harvested after a 6 hour induction at 35 °C and frozen at −80 °C. Protein purification procedure was similar to a previous report [24]. Purified TatB protein in DPC micelles was exchanged into 20 mM sodium acetate buffer (pH 5.5). In the final sample, the molar ratio of protein:DPC was ~1:40.

2.2. Circular dichroism (CD) spectroscopy

The CD spectra were recorded on a Mos-450 spectropolarimeter (Bio-Logic, France) at room temperature. All spectra were collected over a wavelength ranging from 190 nm to 250 nm with a step size of 1 nm using a 0.1 cm optical path length cell. The protein concentrations were about 0.2 mg/mL. Spectra were obtained by averaging three scans for each sample. Data were analyzed using CDPro [25].

2.3. Chemical cross-linking of TatB_{1-101}

The purified TatB$_{1-101}$ (~0.1 mM) was cross-linked by incubating with 2 mM disuccinimidyl suberate (Thermo Scientific, DSS) or 0.1% glutaraldehyde (GA) at room temperature for 10 min under two different DPC concentrations (protein:DPC molar ratio of 1:50 or 1:250), quenched with 50 mM Tris–HCl, pH 8.0, and analyzed by SDS-PAGE.

2.4. NMR spectroscopy

The NMR experiments were performed at 40 °C on Bruker Avance 500, 600, 700 and 800 MHz spectrometers equipped with four RF channels and triple-resonance cryo-probes with pulsed-field gradients. The chemical shift assignments were obtained by conventional triple resonance experiments [26] using a $^{13}C/^{15}N$-labeled TatB$_{1-101}$ sample in perdeuterated DPC micelles. 3D ^{15}N- and ^{13}C-edited NOESY–HSQC spectra (mixing time 100 ms) for TatB$_{1-101}$ in perdeuterated DPC micelles were collected to confirm the assignments and obtain distance restraints.

2.5. RDC measurements

The backbone H–N RDC measurements of *E. coli* TatB$_{1-101}$ were performed using the liquid crystalline phase of G-tetrad DNA at 40 °C [27].

To overcome signal overlap and fast relaxation of the up-field component, the RDCs were obtained by the combination of three sets of experiments. The RDC values of strong and well-resolved peaks were primarily extracted from the differences in ^1H–^{15}N splitting measured by ^1H–^{15}N IPAP-HSQC [28]. The RDC data of overlapping peaks were measured using the HNCO/TROSY–HNCO pair of experiments. The RDC values of the weak signals were measured using the intensity-modulated CE-TROSY experiments [29].

2.6. Structure calculation of TatB

The structure calculation of *E. coli* TatB$_{1-101}$ was carried out using inter-proton NOE-derived distance restraints and dihedral angle restraints. The program TALOS was used to predict dihedral angles ψ and φ restraints [30]. The calculation was carried out using the program CYANA [31]. 100 structures were calculated, and 15 conformers with the lowest total energy were selected to represent the TatB protein. Backbone N–H RDCs were used for structure validation. The fitting of RDCs with the structures was performed by the program PALES using the single value decomposition (SVD) method [32]. The atomic coordinates have been deposited in the Protein Data Bank (PDB ID: 2MI2).

2.7. Backbone dynamics

The backbone ^{15}N relaxation parameters including the longitudinal relaxation rates R_1, the transverse relaxation rates R_2, and the steady-state heteronuclear {^1H}–^{15}N NOE values of TatB$_{1-101}$ were measured [33]. The experiments were performed on a Bruker Avance 800 MHz NMR spectrometer at 40 °C. The delays used for the R_1 experiments were 10 (×2), 100, 200, 300, 400, 600, 800, 1,000, 1,600, 2,400, 3,200 and 4,000 ms, and those used for the R_2 experiments were 7.4 (×2), 14.8, 22.3, 29.7, 37.1, 44.5, 52.0, 66.8, 89.0 and 111.4 ms. The relaxation rate constants were obtained by fitting the peak intensities to a single exponential function using the nonlinear least-squares method as described [34]. The {^1H}–^{15}N NOE experiments were performed in the presence and absence of a 3-s proton pre-saturation period prior to the ^{15}N excitation pulse and using recycle delays of 2 and 5 s, respectively.

3. Results and discussion

3.1. Characterization of E. coli TatB

The *E. coli* TatB protein contains 171 amino acids. Sequence alignment shows that the C-terminal 70 residues are not conserved in Gammaproteobacteria (Fig. 1A). Previous functional assays also suggested that the C-terminal tail is not essential for TatB function, and its truncation does not affect the Tat translocation activity [21]. Therefore, a truncated construct of TatB comprising residues Met1 to Pro101 (termed as TatB$_{1-101}$) was prepared and used throughout this study.

To verify the secondary structure composition of TatB, CD spectrum was recorded for TatB$_{1-101}$ in liposomes (Fig. 1B). The CD spectrum shows that TatB$_{1-101}$ is an α-rich protein, with estimated 52% α-helical and 25% disordered conformations. The CD spectrum of TatB$_{1-101}$ in DPC micelles is almost identical with that in liposomes (Fig. 1B), indicating consistency in secondary structures in the two samples. The results suggest that DPC micelle is a good mimic of membrane environment for structural characterization of TatB.

The ^{15}N-edited heteronuclear single-quantum coherence (HSQC) spectrum of TatB$_{1-101}$ is highly crowded even with the C-terminal region removed. Excluding the C-terminal tag, chemical shift assignments were obtained for all backbone amides except proline residues (Fig. 2). For side chain atoms, 86% of ^{13}C, 47% of ^{15}N and 99% of ^1H chemical shifts were obtained. Analysis of the consensus chemical shift index (CSI) shows that the protein consists of four well-defined helices, comprising
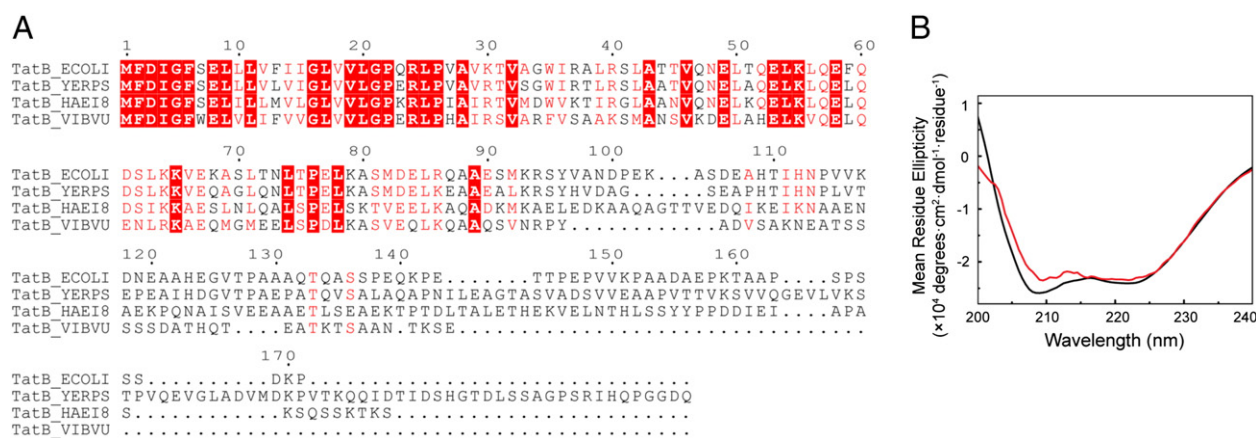
A

B

Fig. 1. Primary and secondary structural analyses of TatB. A) Multiple sequence alignment of TatB proteins from Gammaproteobacteria. The sequences shown are from *E. coli*, *Yersinia pseudotuberculosis*, *Haemophilus influenza*, and *Vibrio vulnificus*. The figure was generated using ESPRIPT [43]. B) CD spectra of TatB$_{1-101}$ in liposomes (red) and DPC micelles (black).

of residues 6–19 (α1), 26–53 (α2), 56–71 (α3) and 77–96 (α4), respectively (Fig. S1). This is consistent with the CD spectrum of TatB$_{1-101}$ in DPC micelles, which also indicates an all-helical conformation.

In addition, we investigated the oligomerization state of the TatB$_{1-101}$ sample by cross-linking using either GA or DSS. A new band corresponding to the dimeric form is observable in the SDS-PAGE,
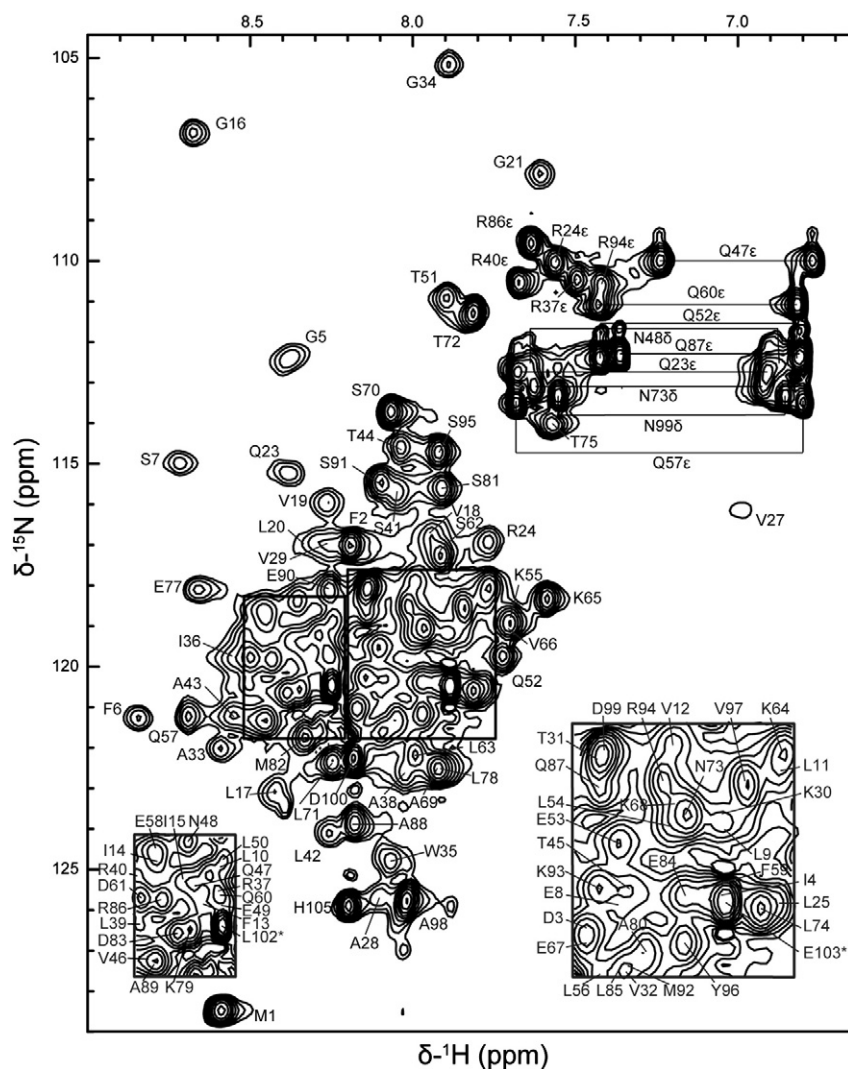

Fig. 2. 2D ^{1}H–^{15}N HSQC spectrum of TatB$_{1-101}$ in DPC micelles annotated with the backbone assignments. The spectrum was collected on a Bruker Avance 800 MHz spectrometer (with a cryo-probe) at 40 °C. The assignments are labeled with the one-letter amino acid code and residue number. The side chain NH$_2$ peaks of Asn and Gln are connected by horizontal lines. The asterisk indicates residues of the His-tag.

whereas the majority of the protein sample remains in the monomeric state (Fig. S2). It is possible that the TatB$_{1-101}$ exists as a mixture of monomer and dimer, and the NMR signals we observed may mostly originate from the monomeric form.

3.2. Solution structure of TatB$_{1-101}$

The structures of TatB$_{1-101}$ were calculated using NOE-derived distance restraints together with dihedral angle and H-bond restraints. The H-bond restraints were derived from the NOE patterns and used only for the α-helical regions. The calculated structures are shown in ensemble and ribbon diagrams (Fig. 3B–C), and the structural statistics are summarized in Table 1. The atomic coordinates have been deposited in the Protein Data Bank (PDB code: 2MI2). All the conformers in the representative ensemble fit well with the RDC data, giving an average correlation coefficient of 0.80.

TatB$_{1-101}$ comprises four well-defined α-helices (Fig. 3C) as indicated from the NOE patterns and the fitting of RDC data to sinusoids (Fig. 3D). Helix α1 (Ser7–Leu19) is highly hydrophobic and corresponds to the transmembrane helix (TMH), helix α2 (Val27–Gln47) is an amphipathic helix (APH), whereas both helices α3 (Leu56–Leu71) and α4 (Glu77–Tyr96) are hydrophilic with over 70% polar and charged residues.

Table 1
Structural statistics of *E. coli* TatB$_{1-101}$.

Experimental restraints	
Total NOE	
Total unambiguous NOE	2294
Intra-residue	880
Inter-residue	1414
Sequential ($|i-j| = 1$)	651
Medium-range ($|i-j| \leq 4$)	708
Long-range ($|i-j| \geq 5$)	47
Total ambiguous NOE	183
Total dihedral angle restraints ($\varphi + \psi$)	139 (69 + 70)
Restraint violations	
Distance restraint violations > 0.3 Å	0
Dihedral angle restraint violations > 5º	0
RMSD[a] from mean structure (Å)	
All heavy atoms	2.6 ± 1.3
All backbone atoms	2.5 ± 1.3
Secondary structure heavy	2.4 ± 1.2
Secondary structure backbone	2.3 ± 1.2
Ramachandran statistics (%)	
Most favored regions	78.9
Additional allowed regions	15.7
Generously allowed regions	4.5
Disallowed regions	0.9

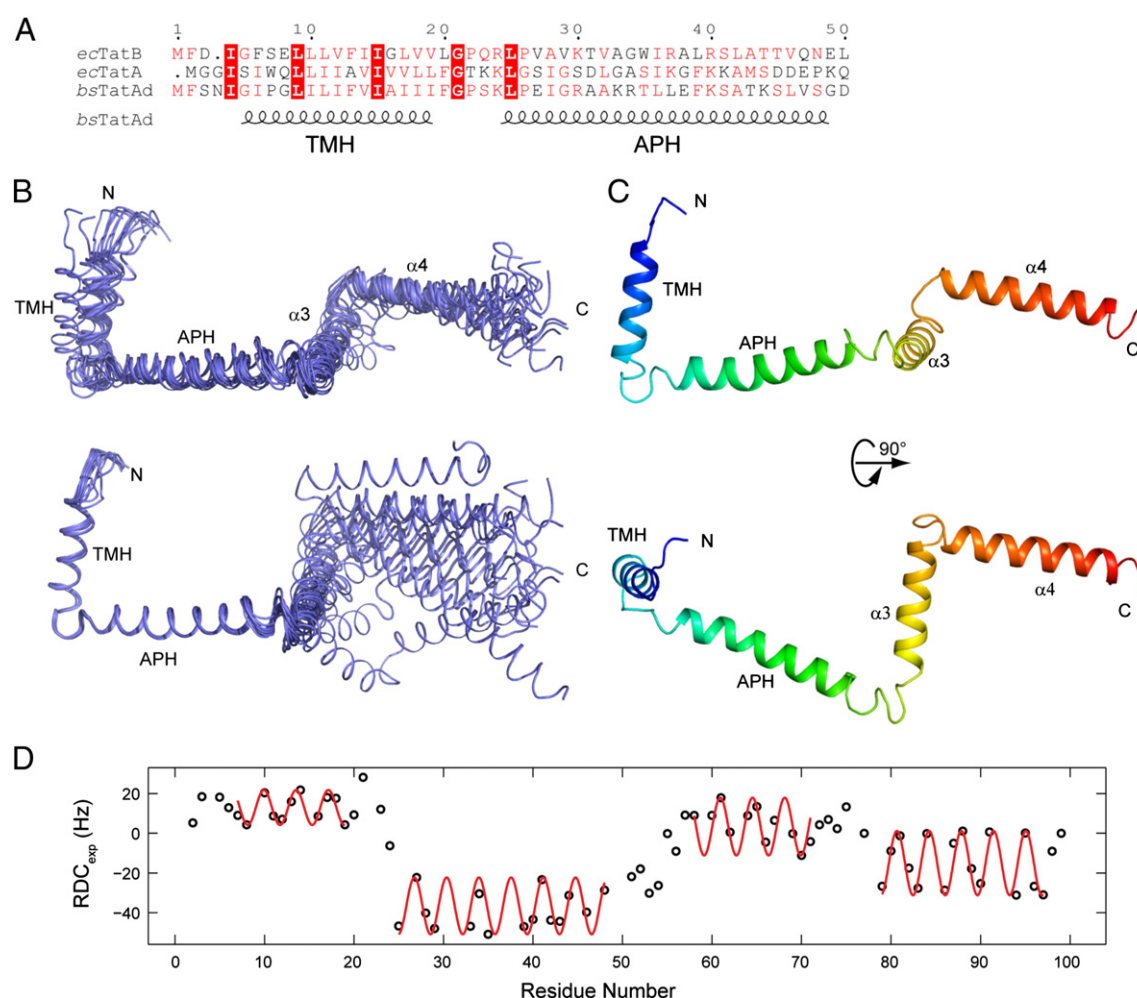[a] The RMSD values of the monomer were calculated for residues 4–98.

Fig. 3. Solution structure of TatB$_{1-101}$ in DPC micelles. A) Multiple sequence alignment of *E. coli* TatB with *E. coli* TatA and *B. subtilis* TatA$_d$, showing only the TMH and APH regions. The figure was generated using ESPRIPT [43]. B) Structure ensemble of the 15 lowest-energy conformers of TatB$_{1-101}$. The conformers are aligned to all secondary backbone atoms (upper) and secondary backbone atoms of residue 6–47 (lower). C) Ribbon diagram representation of TatB$_{1-101}$. D) Backbone N-H RDC values and fitting to sinusoid function using a fixed periodicity of 3.6 (shown in red) [44].

Amides in the TMH show strong NOESY cross-peaks with the aliphatic tails of non-deuterated DPC molecules but have no signals with water, indicating that this helix is buried inside the micelle. Similarly, amides in the linker between TMH and APH show weak cross-peaks with detergent molecules but have no signals with water, suggesting that the linker is buried inside the micelle. However, the side chain amide protons of Gln23 and Arg24 show cross-peaks with both water and detergent, suggesting that these residues are positioned on the water–micelle interface. Moreover, the amides of the APH show cross-peaks to detergent signals, although the intensities are lower compared to the TMH-detergent cross-peaks. In contrast, most residues in the region Leu50–Pro101 are solvent-exposed as indicated by showing strong cross-peaks with water but none with detergent. Based on these observations, only the TMH is inserted into the hydrophobic core of the DPC micelle, the APH lies on the micelle surface, and the rest of the protein is mostly exposed in aqueous solution. This result is consistent with earlier studies using solid-state NMR spectroscopy [35,36].

3.3. TatB₁₋₁₀₁ forms an extended L-shape structure

The linkers between adjacent helices are six to eight residues in length. Notably, all three linkers (residues Leu20–Pro26, Asn48–Lys55, Thr72–Pro76) are highly conserved in the TatB protein family (Fig. 1A). The first linker connecting TMH and APH contains the most conserved 'L-G-P-X-R-L-P' sequence. Twenty-three unique long-range NOEs were observed at this region, particularly between residue pairs Phe13–Leu25, Leu17–Pro22, Leu17–Leu25 and Leu20–Leu25 (Fig. 4A). The APH-α3 linker (N/T-E-L/V-X-Q/H-E-L-K) and α3–α4 linker (L/M-X-X-L-T/S-P) are less conserved compared to the TMH–APH linker in sequence (Fig. 1A), and a total of eleven and thirteen unique long-range NOEs were observed for these two linkers, respectively (Fig. 4B–C).

As is clear from the structure ensemble, the orientation between the TMH and APH helices is relatively rigid (Fig. 3B). The extensive interactions observed at the TMH-APH linker region contribute to the stabilization of the local conformation, and restrict the relative movement between the two helices (Fig. 4A). In comparison, the NOE contacts observed at both APH-α3 and α3–α4 linkers are much fewer, and the local conformations at these two regions are more flexible (Fig. 4B–C). As a result, the structural ensemble of TatB is not well converged, particularly in the α3 and α4 segments (Fig. 3B). When we align the ensemble structures using backbone atoms from all secondary structural elements, the derived root mean square deviation (RMSD) is 2.2 Å. However, if we align only the TMH and APH segments, high structural convergence is observed with a backbone RMSD of only 0.3 Å (Fig. 3B). In addition, fitting the RDC values with the ensemble structures using data from TMH and APH alone shows an average correlation coefficient of 0.89, which is higher than the coefficient value of 0.80

when using data from all four helices. This again supports that the orientation of TMH and APH is better characterized compared to the helices α3 and α4.

Furthermore, we prepared another truncated construct TatB₁₋₇₁, in which helix α4 was also removed. The HSQC spectra of TatB₁₋₁₀₁ and TatB₁₋₇₁ are similar under the same experimental condition (Fig. S3). The exact positions of about one-third of the peaks cannot be analyzed due to severe signal overlap. For well-resolved peaks, the composite chemical shift differences between the two sets of peaks are relatively small (Fig. S4). The most significantly affected region is helix α3. It shows an average chemical shift difference of ~0.05 ppm, which is close to the digital resolution (0.04 ppm). These observations suggest that helix α4 is floppy and does not interact with other regions of the protein, supporting that TatB₁₋₁₀₁ adopts an extended 'L-shape' structure.

3.4. Structural analysis of TatB₁₋₁₀₁

The N-terminal nine residues ('M-F-D-I-G-F-X-E-L') are strictly conserved in the TatB family and are lacking in the paralogous TatA family (Figs. 1A and 3A). This region corresponds to the first turn of the TMH and the N-terminal extended conformation (Fig. 3B). The N-terminal extended segment (residues Met1–Phe6) is relatively rigid, and extends over a length of ~10 Å. The TMH itself is ~20 Å in length. Therefore, segment Met1–Leu19 spans a total of ~30 Å, which is approximately the width of the lipid bilayer. The amides of residue Met1–Gly5 show NOE cross-peaks with both DPC and water, suggesting that these residues are positioned on the micelle–water interface.

Instead of functioning alone, TatB forms a tight complex with TatC at a 1:1 molar ratio [37,38]. Several residues on TatB have been suggested to participate in TatB–TatC interaction: cysteine substitution at Leu9 or Leu10 allows disulfide cross-linking with TatC [20,39]; mutation at Phe6 can suppress an inactivated TatC mutant [39]. These residues mostly locate in the N-terminal region, and cluster at one side of the TMH (Fig. 5B). Besides, cysteine cross-linking experiment demonstrated that TatB forms tetrameric units by self-oligomerization. Residues Leu11 and Ile15 were identified at the oligomeric interface [40]. As shown in Fig. 5B, the residues involving in TatB self-oligomerization and TatB–TatC interaction locate on opposite sides of the TatB TMH.

To better describe the TatB protein, we plotted the electrostatic potential along with amino acid conservation onto the protein structure. The APH contains twenty-one residues, including twelve hydrophobic and six hydrophilic/polar residues. Instead of forming a continuous hydrophobic surface on one side of the helix, the hydrophobic residues cluster into two separate patches (Fig. 5A and D). One locates in the N-terminal half of the APH segment, with their side chains pointing towards the TMH. The other locates in the C-terminal half of APH and is rotated 120° away from the first patch. By analyzing the NOESY
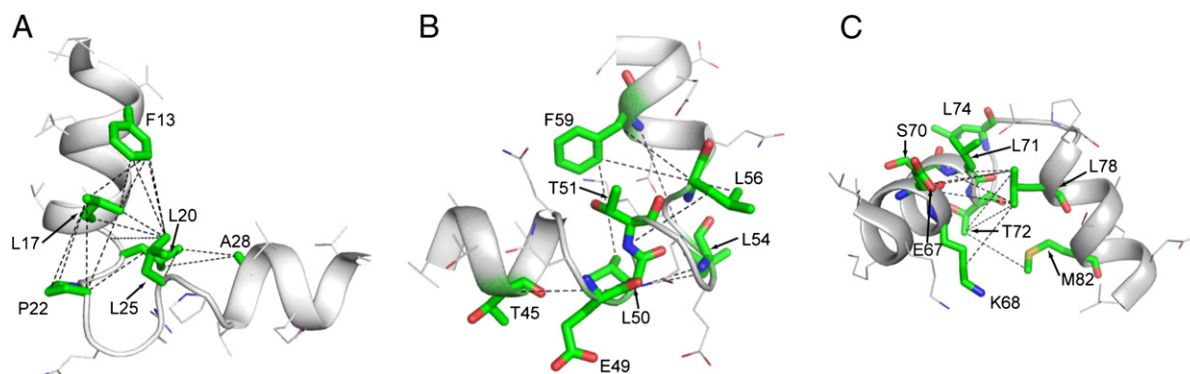

Fig. 4. Linker regions of *E. coli* TatB₁₋₁₀₁. Interaction networks based on ¹H–¹H NOE cross-peaks are shown in dashed lines for the TMH–APH linker (A), APH-α3 linker (B) and α3–α4 linker (C). For clarity, not all observed interactions are shown.
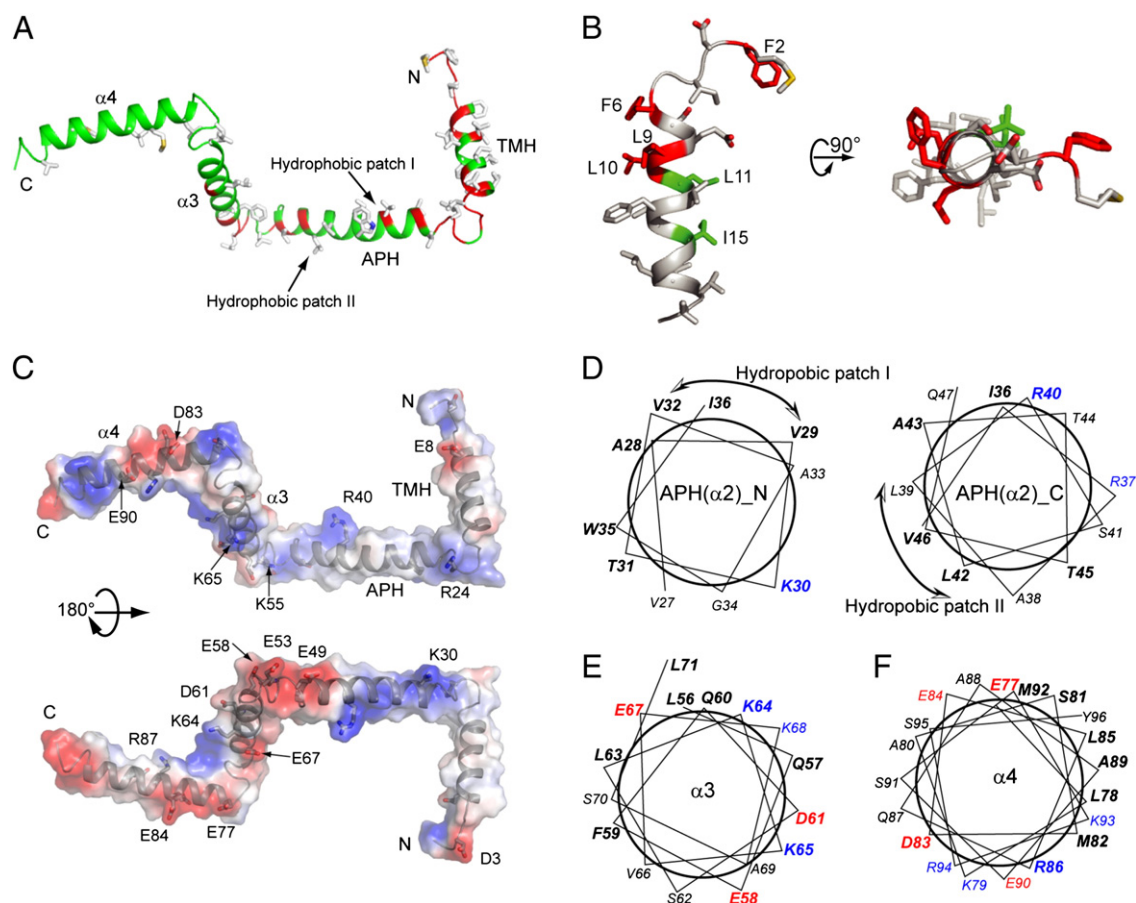
Fig. 5. Structural analysis of TatB$_{1-101}$. A) Ribbon diagram representation of TatB$_{1-101}$ with conserved residues shown in red and hydrophobic residues shown as white sticks. B) Solution structure of the N-terminus and TMH of TatB. Residues identified for interactions with TatC and TatB subunits are shown in red and green, respectively. C) Surface representation of the TatB$_{1-101}$ with electrostatic potential. Side chains of conserved residues are shown in sticks and are labeled. Structure-based helical wheel diagrams of the APH (D), α3 (E) and α4 (F) segments of TatB. The diagrams were generated by an in-house written script using the coordinates of Cα atoms in the solution structure. Positively and negatively charged residues are shown in blue and red, respectively. Conserved residues in TatB family are labeled in bold.

spectra, we observed that residues in the N-terminal part of APH show stronger cross-peaks with detergent molecules than those in the C-terminal part. For residues after Leu42, no NOE cross-peaks with detergent could be observed. This result suggests that the second hydrophobic patch is most likely to be exposed in the aqueous solution.

The APH contains three positively charged residues, Lys30, Arg37 and Arg40. As shown in Fig. 5C, these residues form a continuous positively charged surface along the N-terminal half of APH. Charged residues on APH-α3 linker, especially Glu49 and Glu53, together with polar residues on the C-terminal half of APH, form a negatively charged region. Helices α3 and α4 contain six and eight charged residues respectively (Fig. 5E–F), which is twice as much as in APH. Though rich in charged residues, both helices α3 and α4 have a zero net charge. Interestingly, the charged residues in α3 are generally conserved in the TatB family, whereas those in α4 are not.

3.5. Conformational dynamics of TatB

The TatB protein adopts an extended conformation with four helices connected by relatively flexible linkers. To characterize the dynamic properties of TatB, we measured the backbone relaxation rates R_1, R_2 and {^{1}H}–^{15}N heteronuclear NOE values by solution NMR spectroscopy (see Materials and methods). In general, the value of {^{1}H}–^{15}N NOE can be used as an indication of structural flexibility in the ps–ns timescales, with higher values corresponding to a more ordered conformation. The R_2/R_1 ratio can be used to estimate the global correlation time of the molecule and identify residues undergoing chemical/conformational exchanges on the μs–ms timescales [41]. However, the R_2/R_1 ratio is also highly sensitive to motional anisotropy, which is difficult to be separated from chemical/conformational exchanges. In contrast, the $R_1 \cdot R_2$ values are not affected by motional anisotropy and can be used to analyze chemical/conformational exchanges [42].

The relaxation parameters measured for TatB$_{1-101}$ are shown in Fig. 6. The {^{1}H}–^{15}N NOE values for residues in the four helices are notably higher than those in the linkers and N- and C-termini. The TMH shows the highest average {^{1}H}–^{15}N NOE value of ~0.74 (Fig. 6), whereas the average {^{1}H}–^{15}N NOE value for APH is slightly decreased (~0.70). The average values for helices α3 and α4 are even lower (~0.64). These data suggest that the flexibility in the helical segments gradually increase toward the C-terminal. This is consistent with the structural feature that helices α3 and α4 are floppy and do not show a converged conformation in the structure ensemble.

Residues in the TMH and APH show apparently higher R_2/R_1 ratios, consistent with the notion that these two helices are associated with the DPC micelle (Fig. 6). The lower R_2/R_1 ratios of residues in helices α3 and α4 reflect a smaller overall correlation time, which again supports that the motions of the two helices are independent to the micelle. The overall $R_1 \cdot R_2$ values are similar for the four helices, whereas the values observed at the APH-α3 linker are notably higher (Fig. 6). This suggests that the APH-α3 linker may undergo conformational exchanges in the μs–ms timescales. This is consistent with the solution structure, in which APH and α3 do not have fixed orientations.
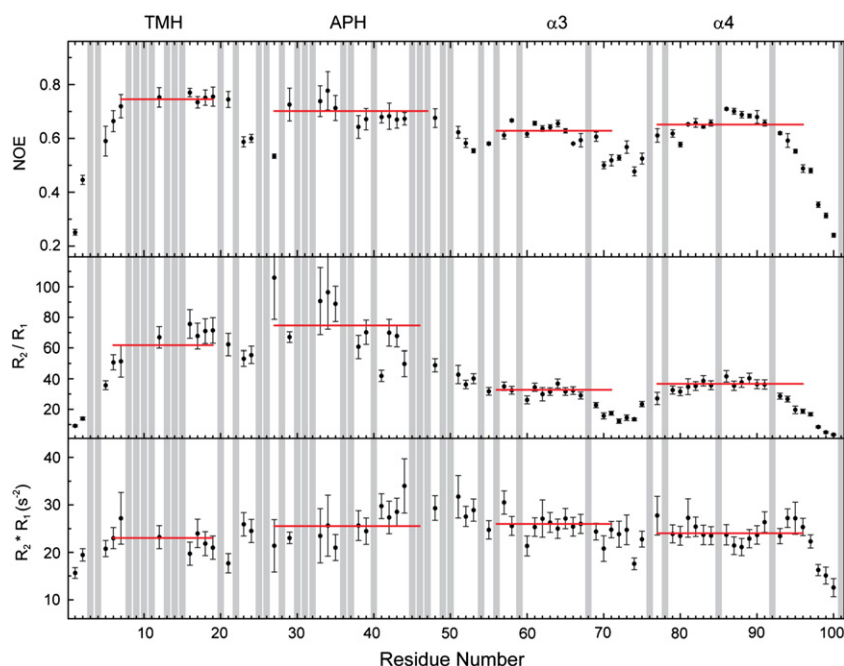
Fig. 6. Backbone dynamics of *E. coli* $TatB_{1-101}$. The backbone ^{15}N relaxation parameters of TatB protein, including the steady-state heteronuclear $\{^1H\} - ^{15}N$ NOE values, the R_2/R_1 and R_1*R_2 values as a function of residue numbers. The red line indicates the average value of each helix. The gray shadow indicates residues with signal overlaps.

Evidences suggest that TatB functions to prevent premature signal peptide cleavage [23]. Biochemical studies revealed that residues Leu9, Gly34, Trp35, Ile36, Leu54, Leu56 and Leu78 of TatB are in close vicinity with the substrate protein during translocation [22]. Residues Trp35 and Ile36 are located at the beginning of hydrophobic patch II on APH and are partially exposed in the aqueous solution, favoring interaction with the substrate. Residues Leu54, Leu56 and Leu78 are located in the flexible regions including helices α3 and α4. Therefore, the residues contributing to substrate interactions scatter in different regions of the TatB protein and are able to sample a large conformational space (Fig. 7). A possible scenario is that the floppy helices change their relative orientations by the flexible movements at the linkers and wrap around the substrate proteins to facilitate binding (Fig. 7). The observed mobility of the last two helices may play an important role in adapting to substrate proteins with various sizes and shapes.
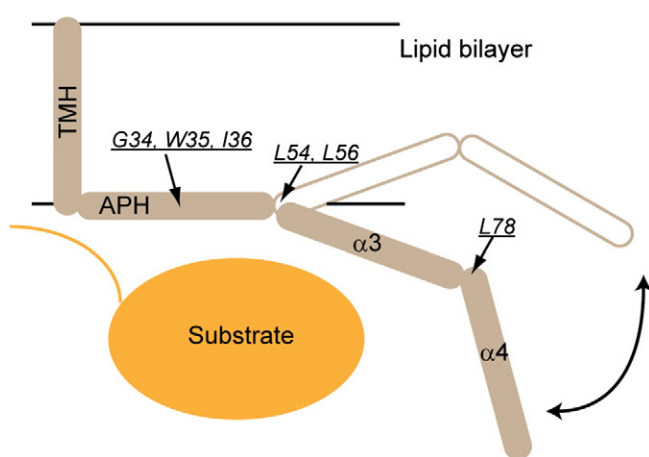
4. Conclusion

In summary, we have determined the solution structure of TatB in DPC micelles by NMR spectroscopy. TatB consists of four α-helices and adopts an extended L-shape conformation. The TMH and APH segments are relatively rigid, while helices α3 and α4 show higher mobility. Our structural and dynamic results provide implications for TatB function. In particular, the observed high flexibility in helices α3 and α4 sheds new light on the mechanism for the Tat system in recognizing and translocating folded proteins of various sizes and shapes. Further investigations under closer-to-native conditions (i.e. in the presence of TatC and with natural phospholipids) would be necessary for a deeper understanding of the conformational landscape of TatB during protein translocation.

Appendix A. Supplementary data

Supplementary data to this article can be found online at http://dx. doi.org/10.1016/j.bbamem.2014.03.015.

Fig. 7. Model of TatB–substrate interactions. A model of TatB interaction with the substrate protein. Residues identified for interaction with substrate proteins are labeled.

References

[1] A.J. Driessen, N. Nouwen, Protein translocation across the bacterial cytoplasmic membrane, Annu. Rev. Biochem. 77 (2008) 643–667.

[2] T. Palmer, B.C. Berks, The twin-arginine translocation (Tat) protein export pathway, Nat. Rev. Microbiol. 10 (2012) 483–496.

[3] J. Frobel, P. Rose, M. Muller, Twin-arginine-dependent translocation of folded proteins, Philos. Trans. R. Soc. B 367 (2012) 1029–1046.

[4] E. De Buck, E. Lammertyn, J. Anne, The importance of the twin-arginine translocation pathway for bacterial virulence, Trends Microbiol. 16 (2008) 442–453.

[5] U. Gohlke, L. Pullan, C.A. McDevitt, I. Porcelli, E. de Leeuw, T. Palmer, H.R. Saibil, B.C. Berks, The TatA component of the twin-arginine protein transport system forms channel complexes of variable diameter, Proc. Natl. Acad. Sci. U. S. A. 102 (2005) 10482–10486.

[6] M.C. Leake, N.P. Greene, R.M. Godun, T. Granjon, G. Buchanan, S. Chen, R.M. Berry, T. Palmer, B.C. Berks, Variable stoichiometry of the TatA component of the twin-arginine protein transport system observed by in vivo single-molecule imaging, Proc. Natl. Acad. Sci. U. S. A. 105 (2008) 15376–15381.

[7] F. Alcock, M.A.B. Baker, N.P. Greene, T. Palmer, M.I. Wallace, B.C. Berks, Live cell imaging shows reversible assembly of the TatA component of the twin-arginine protein transport system, Proc. Natl. Acad. Sci. U. S. A. 110 (2013) E3650–3659 (in press).

[8] F. Rodriguez, S.L. Rouse, C.E. Tait, J. Harmer, A. De Riso, C.R. Timmel, M.S. Sansom, B.C. Berks, J.R. Schnell, Structural model for the protein-translocating element of the twin-arginine transport system, Proc. Natl. Acad. Sci. U. S. A. 110 (2013) E1092–E1101.

[9] E.M. Strauch, G. Georgiou, *Escherichia coli* tatC mutations that suppress defective twin-arginine transporter signal peptides, J. Mol. Biol. 374 (2007) 283–291.

[10] S. Ramasamy, R. Abrol, C.J. Suloway, W.M. Clemons Jr., The glove-like structure of the conserved membrane protein TatC provides insight into signal sequence recognition in twin-arginine translocation, Structure 21 (2013) 777–788.

[11] F. Sargent, N.R. Stanley, B.C. Berks, T. Palmer, Sec-independent protein translocation in *Escherichia coli*. A distinct and pivotal role for the TatB protein, J. Biol. Chem. 274 (1999) 36073–36082.

[12] A. Bolhuis, J.E. Mathers, J.D. Thomas, C.M. Barrett, C. Robinson, TatB and TatC form a functional and structural unit of the twin-arginine translocase from *Escherichia coli*, J. Biol. Chem. 276 (2001) 20213–20219.

[13] G.L. Orriss, M.J. Tarry, B. Ize, F. Sargent, S.M. Lea, T. Palmer, B.C. Berks, TatBC, TatB, and TatC form structurally autonomous units within the twin arginine protein transport system of *Escherichia coli*, FEBS Lett. 581 (2007) 4091–4097.

[14] M.J. Tarry, E. Schafer, S.Y. Chen, G. Buchanan, N.P. Greene, S.M. Lea, T. Palmer, H.R. Saibil, B.C. Berks, Structural analysis of substrate binding by the TatBC component of the twin-arginine protein transport system, Proc. Natl. Acad. Sci. U. S. A. 106 (2009) 13284–13289.

[15] K. Cline, H. Mori, Thylakoid ΔpH-dependent precursor proteins bind to a *cp*TatC-Hcf106 complex before Tha4-dependent transport, J. Cell Biol. 154 (2001) 719–729.

[16] F. Gerard, K. Cline, The thylakoid proton gradient promotes an advanced stage of signal peptide binding deep within the Tat pathway receptor complex, J. Biol. Chem. 282 (2007) 5263–5272.

[17] S. Panahandeh, C. Maurer, M. Moser, M.P. DeLisa, M. Muller, Following the path of a twin-arginine precursor along the TatABC translocase of *Escherichia coli*, J. Biol. Chem. 283 (2008) 33267–33275.

[18] K. Cline, M. McCaffery, Evidence for a dynamic and transient pathway through the TAT protein transport machinery, EMBO J. 26 (2007) 3039–3049.

[19] H. Mori, K. Cline, A twin arginine signal peptide and the pH gradient trigger reversible assembly of the thylakoid ΔpH/Tat translocase, J. Cell Biol. 157 (2002) 205–210.

[20] S.E. Rollauer, M.J. Tarry, J.E. Graham, M. Jaaskelainen, F. Jager, S. Johnson, M. Krehenbrink, S.-M. Liu, M.J. Lukey, J. Marcoux, M.A. McDowell, F. Rodriguez, P. Roversi, P.J. Stansfeld, C.V. Robinson, M.S.P. Sansom, T. Palmer, M. Hogbom, B.C. Berks, S.M. Lea, Structure of the TatC core of the twin-arginine protein transport system, Nature 492 (2012) 210–214.

[21] S. Koch, M.J. Fritsch, G. Buchanan, T. Palmer, *Escherichia coli* TatA and TatB proteins have N-out, C-in topology in intact cells, J. Biol. Chem. 287 (2012) 14420–14431.

[22] C. Maurer, S. Panahandeh, A.C. Jungkamp, M. Moser, M. Muller, TatB functions as an oligomeric binding site for folded Tat precursor proteins, Mol. Biol. Cell 21 (2010) 4151–4161.

[23] J. Frobel, P. Rose, F. Lausberg, A.S. Blummel, R. Freudl, M. Muller, Transmembrane insertion of twin-arginine signal peptides is driven by TatC and regulated by TatB, Nat. Commun. 3 (2012) 1311.

[24] Y. Hu, E. Zhao, H. Li, B. Xia, C. Jin, Solution NMR structure of the TatA component of the twin-arginine protein transport system from gram-positive bacterium *Bacillus subtilis*, J. Am. Chem. Soc. 132 (2010) 15942–15944.

[25] N. Sreerama, R.W. Woody, Estimation of protein secondary structure from circular dichroism spectra: comparison of CONTIN, SELCON, and CDSSTR methods with an expanded reference set, Anal. Biochem. 287 (2000) 252–260.

[26] M. Sattler, J. Schleucher, C. Griesinger, Heteronuclear multidimensional NMR experiments for the structure determination of proteins in solution employing pulsed field gradients, Prog. Nucl. Magn. Reson. Spectrosc. 34 (1999) 93–158.

[27] J. Lorieau, L. Yao, A. Bax, Liquid crystalline phase of G-tetrad DNA for NMR study of detergent-solubilized proteins, J. Am. Chem. Soc. 130 (2008) 7536–7537.

[28] M. Ottiger, F. Delaglio, A. Bax, Measurement of J and dipolar couplings from simplified two-dimensional NMR spectra, J. Magn. Reson. 131 (1998) 373–378.

[29] N.U. Jain, S. Noble, J.H. Prestegard, Structural characterization of a mannose-binding protein-trimannoside complex using residual dipolar couplings, J. Mol. Biol. 328 (2003) 451–462.

[30] G. Cornilescu, F. Delaglio, A. Bax, Protein backbone angle restraints from searching a database for chemical shift and sequence homology, J. Biomol. NMR 13 (1999) 289–302.

[31] P. Guntert, C. Mumenthaler, K. Wuthrich, Torsion angle dynamics for NMR structure calculation with the new program DYANA, J. Mol. Biol. 273 (1997) 283–298.

[32] M. Zweckstetter, NMR: prediction of molecular alignment from structure using the PALES software, Nat. Protoc. 3 (2008) 679–690.

[33] N.A. Farrow, R. Muhandiram, A.U. Singer, S.M. Pascal, C.M. Kay, G. Gish, S.E. Shoelson, T. Pawson, J.D. Forman-Kay, L.E. Kay, Backbone dynamics of a free and phosphopeptide-complexed Src homology 2 domain studied by [15] N NMR relaxation, Biochemistry 33 (1994) 5984–6003.

[34] D. Fushman, S. Cahill, D. Cowburn, The main-chain dynamics of the dynamin pleckstrin homology (PH) domain in solution: analysis of [15] N relaxation with monomer/dimer equilibration, J. Mol. Biol. 266 (1997) 173–194.

[35] L. Zhang, L. Liu, S. Maltsev, G.A. Lorigan, C. Dabney-Smith, Solid-state NMR investigations of peptide—lipid interactions of the transmembrane domain of a plant-derived protein, Hcf106, Chem. Phys. Lipids 175–176 (2013) 123–130.

[36] L. Zhang, L. Liu, S. Maltsev, G.A. Lorigan, C. Dabney-Smith, Investigating the interaction between peptides of the amphipathic helix of Hcf106 and the phospholipid bilayer by solid-state NMR spectroscopy, Biochim. Biophys. Acta 1838 (2014) 413–418.

[37] P.A. Lee, G. Buchanan, N.R. Stanley, B.C. Berks, T. Palmer, Truncation analysis of TatA and TatB defines the minimal functional units required for protein translocation, J. Bacteriol. 184 (2002) 5871–5879.

[38] N. Blaudeck, P. Kreutzenbeck, M. Muller, G.A. Sprenger, R. Freudl, Isolation and characterization of bifunctional *Escherichia coli* TatA mutant proteins that allow efficient tat-dependent protein translocation in the absence of TatB, J. Biol. Chem. 280 (2005) 3426–3432.

[39] H. Kneuper, B. Maldonado, F. Jager, M. Krehenbrink, G. Buchanan, R. Keller, M. Muller, B.C. Berks, T. Palmer, Molecular dissection of TatC defines critical regions essential for protein transport and a TatB–TatC contact site, Mol. Microbiol. 85 (2012) 945–961.

[40] P.A. Lee, G.L. Orriss, G. Buchanan, N.P. Greene, P.J. Bond, C. Punginelli, R.L. Jack, M.S.P. Sansom, B.C. Berks, T. Palmer, Cysteine-scanning mutagenesis and disulfide mapping studies of the conserved domain of the twin-arginine translocase TatB component, J. Biol. Chem. 281 (2006) 34072–34085.

[41] L.E. Kay, D.A. Torchia, A. Bax, Backbone dynamics of proteins as studied by [15] N inverse detected heteronuclear NMR spectroscopy: application to staphylococcal nuclease, Biochemistry 28 (1989) 8972–8979.

[42] J.M. Kneller, M. Lu, C. Bracken, An effective method for the discrimination of motional anisotropy and chemical exchange, J. Am. Chem. Soc. 124 (2002) 1852–1853.

[43] P. Gouet, E. Courcelle, D.I. Stuart, F. Metoz, ESPript: analysis of multiple sequence alignments in PostScript, Bioinformatics 15 (1999) 305–308.

[44] M.F. Mesleh, S.J. Opella, Dipolar waves as NMR maps of helices in proteins, J. Magn. Reson. 163 (2003) 288–299